Research Article | Vol. 12, No. 9 / 1 Sep 2022 / Optical Materials Express 3543
Optical Materials EXPRESS

# High-order harmonic spectroscopy of polycrystalline graphene

ROBERTO BOYERO-GARCÍA,* ANA GARCÍA-CABRERA, OSCAR ZURRÓN-CIFUENTES, CARLOS HERNÁNDEZ-GARCÍA, AND LUIS PLAJA

*Grupo de Investigación en Aplicaciones del Láser y Fotónica, Departamento de Física Aplicada, Universidad de Salamanca, E- 37008, Salamanca, Spain*
*robertobg@usal.es*

**Abstract:** Present mass production of large-area single-layer graphene relies fundamentally on chemical vapor deposition methods. The generation of grain boundaries, which divides the sample into a set of crystalline domains, is inherent to these fabrication methods. Recent studies have demonstrated a strong anisotropy in the ultrafast non-linear response of single-layer graphene when subjected to non-perturbative, intense laser fields below the damage threshold. We propose to exploit this anisotropy to characterize the size distribution of graphene domains in polycrystals via high-order harmonic polarimetry. Our simulation results demonstrate the sensitivity of the harmonic polarization state to details of the polycrystal grain distribution. In particular, we show that the rotation in the polarization tilt of the highest-order harmonics holds information about the grain distribution in the polycrystal. As a proof-of-concept, we propose a method to determine the standard deviation of the grain size distribution from the values of the most frequent grain size and the standard deviation of the harmonic tilt rotation from a set of hypothetical measurements on different polycrystal realizations. Our work reveals the capability of high-order harmonic polarimetry to characterize polycrystalline two-dimensional materials.



## 1. Introduction

Single-layer graphene (SLG) is a two dimensional –atomic thin– carbon allotrope with extraordinary potential in a variety of fields, ranging from biomedicine to sensors and microelectronics [1]. Industrial applications require large layers of graphene. Chemical vapor deposition (CVD) on metal substrates is one of the most popular choices to fabricate large-area SLG [2]. However, CVD typically leads to polycrystals with grain size and orientation distributions that depend on the fabrication parameters (substrate, growth temperature, hydrogen flow, etc.) [3]. While graphene's electronic properties are degraded by the grain boundaries [4], the smaller fraction of the boundary regions against the total grain surface makes the optical response to be dominated by the inner part of the grain [3]. Grain analysis can be performed using a variety of techniques, either resolving the grain scale (using transmission electron microscopy [3]) or the polycrystal scale (using low-energy electron microscopy [5] or by Raman microscopy [6]).

High-order harmonic generation (HHG) stands as a unique method to produce short-wavelength coherent radiation. This highly non-linear process is triggered by the intense laser-matter interaction driven mainly by infrared and mid-infrared laser pulses. As a result, high-order harmonics of the driving field, extending towards the extreme-ultraviolet or even soft x-rays, are produced [7]. The extraordinary coherence of the process allows tracking the fastest laser-driven electronic dynamics at the attosecond timescales [8]. While HHG was initially explored using gaseous targets [9,10], a substantial interest has recently burgeoned its study in crystalline solids [11].

#468125 https://doi.org/10.1364/OME.468125
Journal © 2022 Received 16 Jun 2022; revised 30 Jul 2022; accepted 1 Aug 2022; published 10 Aug 2022

Optical Materials EXPRESS

The underlying mechanism of HHG in two-dimensional (2D) solids depends strongly on the interaction geometry. On the one hand, for intense p-polarized driving fields at grazing incidence, the process resembles that reported for atoms and molecules [12]: electrons are detached from the crystal's surface, quiver in the continuum, and are finally redirected to collide with the crystal potential, where harmonics are emitted [13]. Interestingly, the detached electron wavefunction preserves the transverse structure imprinted by the crystal potential. These transverse modulations introduce a Talbot revival dynamics at the femtosecond/nanometer scale, whose signature can be resolved in the harmonic spectrum [14]. On the other hand, at normal incidence, the electrons remain in the crystal plane. In such scenario, the driving field generates electron-hole pairs from tunneling excitation at the band gap. Once excited, electrons and holes quiver in reciprocal space following corresponding trajectories in direct space. The harmonic emission occurs from pair recombination when the electron and hole trajectories overlap [15,16], or when they are sufficiently close [17,18]. The corresponding mechanism of HHG in single-layer graphene differs from finite gap solids in the very first step, in which excitation results from the non-adiabatic crossings near the Dirac points [19], instead of tunneling. HHG from other carbon allotropes can be understood through modifications of this basic mechanism [20].

The dynamical details of the coupling of the driving field with the crystal structure (energy dispersion or symmetries) introduce time-resolved signatures in the HHG spectra, that can be unraveled using high-harmonic spectroscopy techniques [21]. Among them, it has been recently demonstrated that crystal symmetries introduce an anisotropic nonlinear response [22–25]. In particular, HHG in graphene yields elliptically polarized harmonics when driven by linearly polarized laser pulses, and viceversa [26–28]. In the recent years, these results have triggered the use of the polarization state of the harmonics as an extension to state-of-the-art high harmonic spectroscopic techniques [29]. Consequently, non-linear optics is at the root of recent proposals for the characterization of 2D or quasi-2D materials [30]. While second harmonic spectroscopy and four-wave mixing are used to determine the number of layers, crystal axis orientation and crystal phase and defects, HHG has been demonstrated to be sensitive to crystal orientation, interlayer coupling and valley structure [31].

In this paper we propose to exploit the graphene's non-linear anisotropic response to characterize the statistical distribution of the domain sizes in polycrystalline graphene. For this purpose, we have implemented HHG simulations in polycrystalline graphene based on the time-dependent Schrödinger equation. We have performed a series of calculations of different polycrystal realizations corresponding to a given grain size and orientation distributions, interacting with a mid-infrared linearly-polarized driving field. For each of these realizations, we compute the polarization properties of the generated harmonics. The statistical analysis for a sufficiently large number of polycrystal calculations shows that the harmonics are emitted with zero mean ellipticity and null rotation of the polarization axis, i.e. the average polarization properties of the harmonics reproduce that of the driving field's. However, we show that the standard deviation of these quantities is sensitive to the grain size distribution. From this, we propose a scheme for the characterization of the grain size distribution knowing the most-frequent grain size and the standard deviation of a series of measurements of the harmonic polarization tilt rotation, as measured from a sample of polycrystals.

## 2. Theoretical description of HHG in polycristalline single-layer graphene

We consider polycrystal parameters similar to the corresponding to CVD graphene grown on copper films (see method A in [3]). The polycrystal layer is irradiated by a linearly polarized laser pulse centered at 3 $\mu$m in wavelength and modeled by a $\sin^2$ envelope of 28 fs full width at half maximum (FWHM) in intensity, and peak intensity of $5 \times 10^{11}$ W/cm$^2$ (see Fig. 1a). Each polycrystal presents a typical area of 4.9 $\mu m^2$ and is composed by domains whose size and orientation distributions are plotted in Fig. 1, according to Ref. [3]: panel (b) shows the

Optical Materials EXPRESS

grain's size distribution, the most frequent size being 25 nm, with a standard deviation of 275.8 nm, calculated from the best fit to a Gaussian distribution. The black solid line depicts the Gaussian distribution corresponding to the values extracted from the proof-of-principle proposal described in next section. Panels (c) and (d) depict the distribution of the orientation shift between neighboring domains, and the corresponding absolute orientations of the domains in the polycrystal, respectively. The laser beam is aimed perpendicularly to the sample, and we consider the driver's waist larger than the polycrystal size, therefore the driver's intensity profile can be approximated as constant. Note that this is crucial to ensure that all domains are subjected to the same driving field conditions.

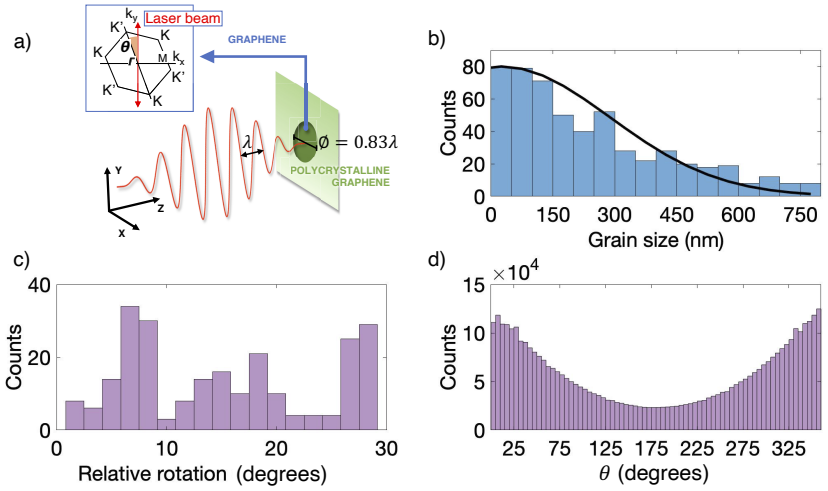


**Fig. 1.** a) Scheme of the interaction between the driving field and a polycrystal. The driving laser is aimed perpendicularly to the graphene's surface, linearly polarized along the y-axis. The inset represents the first Brillouin Zone of graphene, tilted by an angle $\theta$ from the vertical axis, i.e. the driving field's polarization direction. b) Distribution of grain sizes and c) relative grain rotation angles of a polycrystalline graphene grown with CVD, according to [3]. We include in b) the Gaussian distribution resulting from our analysis in section 3. d) Distribution of the absolute angles of rotation of the domains.

Graphene's nonlinear response to intense laser radiation is computed from the integration of the dynamical equations of SLG in the nearest neighbor tight-binding approximation [32]. Following [19] we solve the equations in the oscillatory frame $\boldsymbol{\kappa}_t = \hbar\mathbf{k} - q_e\boldsymbol{\alpha}(t)/c$, where $\mathbf{k}$ are points in the Brillouin Zone, $q_e$ is the electron's charge and $\boldsymbol{\alpha}(t)/c$ is the normalized vector potential of the driving field. Projecting the wavefunction on the Bloch basis of each graphene sublattice ($A$ and $B$), $\{\phi^A_{\mathbf{k}}, \phi^B_{\mathbf{k}}\}$, the light-induced dipole can be computed as [19]

$$\mathbf{d}(t) = \langle\Psi(t)|q_e\mathbf{r}|\Psi(t)\rangle = i\frac{q_e}{2}\int \left[C^*_A(\boldsymbol{\kappa}_t, t)\nabla_{\mathbf{k}}C_A(\boldsymbol{\kappa}_t, t) + C_B(\boldsymbol{\kappa}_t, t)\nabla_{\mathbf{k}}C_B(\boldsymbol{\kappa}_t, t)\right] d\mathbf{k}, \qquad (1)$$

where $C_{A,B}$ are the probability amplitudes of the electron wavefunction in each Bloch basis. The harmonic emission is then calculated from the the dipole acceleration, $\mathbf{a}(t) = \frac{d^2}{dt^2}\mathbf{d}(t)$.

We consider first a set of polycrystals, each built by tiling randomly chosen domains according to the size and orientation distributions shown in Figs. 1(b) to 1c, similar to those reported in [3]. The driving field is linearly polarized along the vertical direction. Therefore, the domain orientation refers to the angle between the grain's $\Gamma - K'$ axis and the vertical axis. If we consider a particular polycrystal realization $j$ in the set, its harmonic emission is computed from the coherent addition of the contributions of the grains. Thus, the $j$-th polycrystal's dipole

Optical Materials EXPRESS

acceleration is computed as $\mathbf{A}_j(t) = \sum_i^{N_j} \mathbf{a}_i(t)$, where $N_j$ is the number of grains and $\mathbf{a}_i(t)$ is the dipole acceleration in each grain, given by the second derivative of Eq. (1).

We compute the harmonic emission from the $j$-th polycrystal through the Fourier transform, $\tilde{\mathbf{A}}_j(\omega)$, of the dipole acceleration $\mathbf{A}_j(t)$. Additionally, we determine the polarization state of the harmonics radiated by the $j$-th polycrystal by calculating the Stokes parameters, $S_k^j(\omega)$, with $k = 0, \ldots, 3$, for each of the Fourier amplitudes $\tilde{\mathbf{A}}_j(\omega)$, as

$$S_0^j(\omega) = \left|\tilde{\mathbf{A}}_{j,\mathbf{x}}(\omega)\right|^2 + \left|\tilde{\mathbf{A}}_{j,\mathbf{y}}(\omega)\right|^2, \tag{2}$$

$$S_1^j(\omega) = \left|\tilde{\mathbf{A}}_{j,\mathbf{x}}(\omega)\right|^2 - \left|\tilde{\mathbf{A}}_{j,\mathbf{y}}(\omega)\right|^2, \tag{3}$$

$$S_2^j(\omega) = \left|\tilde{\mathbf{A}}_{j,\mathbf{a}}(\omega)\right|^2 - \left|\tilde{\mathbf{A}}_{j,\mathbf{b}}(\omega)\right|^2, \tag{4}$$

$$S_3^j(\omega) = \left|\tilde{\mathbf{A}}_{j,\mathbf{r}}(\omega)\right|^2 - \left|\tilde{\mathbf{A}}_{j,\mathbf{l}}(\omega)\right|^2, \tag{5}$$

where ($\mathbf{x}$,$\mathbf{y}$) is the Cartesian basis, ($\mathbf{a}$,$\mathbf{b}$) the 45° rotated basis and ($\mathbf{l}$,$\mathbf{r}$) the circular basis of the space of Jones vectors.

We define the Stokes parameters $S_{q,k}^j$ for a given harmonic order, $q$, as the integral of $S_k^j(\omega)$ along the interval $\Delta\omega = \pm\omega_0/10$ centered at $q\omega_0$, $\omega_0$ being the driving field's frequency. The ellipticity of each harmonic order and the tilt angle of the major axis is then determined from the Stokes parameters as,

$$\epsilon_q^j = \tan\left[\frac{1}{2}\arctan\left(\frac{S_{q,3}^j}{\sqrt{S_{q,1}^{j^2} + S_{q,2}^{j^2}}}\right)\right], \tag{6}$$

$$\theta_q^j = \frac{\pi}{2} - \frac{1}{2}\arctan\frac{S_{q,2}^j}{S_{q,1}^j}. \tag{7}$$

The characterization of the polycrystal domain-size distribution is done considering a set of $8 \times 10^4$ individual polycrystal realizations according to the distributions shown in Fig. 1. The domain rotation is discretized in steps of one degree, and the size distribution in steps of 10 nm. Therefore the number of different domain configurations corresponding to the case of Fig. 1 is about 29000. From each realization, $j$, we compute the high-order harmonic spectrum, and the ellipticity and the tilt of the different harmonic orders. Finally, we derive statistics of the polarization parameters $\epsilon_q^j$ and $\theta_q^j$ (mean and deviation), by collecting the results from the complete set of polycrystal realizations.

## 3. Results and discussion

Figure 2(a) shows the comparison of the harmonic spectrum emitted by a single crystal with that corresponding to a particular polycrystal random realization, $j$. Note that the harmonic spectrum includes little information on the polycrystal structure. This can be understood since, as it has been recently reported in [27], the efficiency of the higher-order harmonic emission is optimal for graphene rotated $15° + k30°$ $\{k \in \mathbb{Z}\}$ from the driver's polarization axis, dominating over the other orientations. In addition, for the lower-order harmonics, the emission is almost insensitive to the orientation. Due to these reasons and, since the domain orientations span over the whole circle (see Fig. 1(d)), the polycrystal harmonic spectrum barely deviates from that of a single crystal oriented with the driver's polarization axis. Therefore, as first conclusion, monitoring the variations of the harmonic efficiency does not result in an useful strategy for the spectroscopic characterization of the polycrystal grain distribution.

An alternative and more successful strategy for the characterization of the polycristal domain distribution consists in looking at the polarization properties of the generated harmonics, instead

Optical Materials EXPRESS

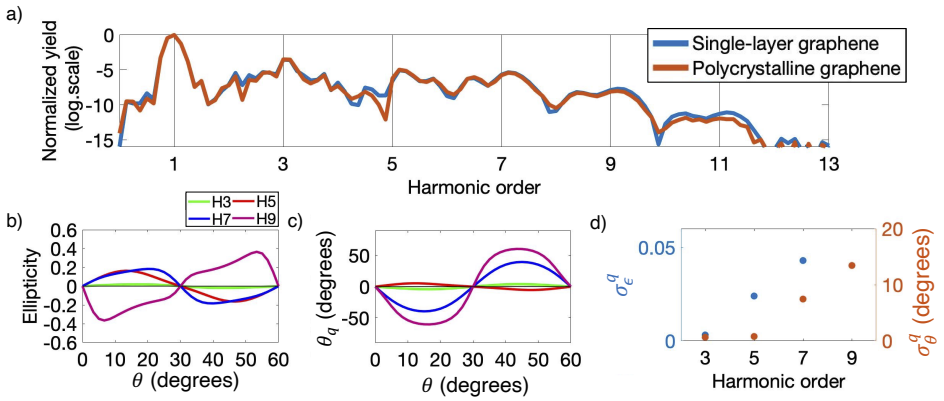


**Fig. 2.** a) Comparison between the spectra of single-crystal graphene (blue line) and that of a particular realization $j$ of a polycrystal (orange line) according to the domain distributions in Fig. 1. b) and c) show the ellipticity and tilt-angle for harmonics 3th to 9th from a single-crystal graphene in terms of the rotation $\theta$ of its $\Gamma - K'$ axis. d) Statistical analysis of the standard deviation of the ellipticity $\sigma_\epsilon^q$ (blue dots) and tilt-angle $\sigma_\theta^q$ (orange dots) for $8 \times 10^4$ polycrystal cases with the distributions shown in Fig. 1.

of at the harmonic efficiency. Our computations show that the polarization of the high-order harmonic emission is indeed sensitive to the domain distribution. This stems from the non-linear anisotropy of single-crystal graphene [27]. Figures 2(b) and 2(c) show the dependence of the ellipticity, $\epsilon_q$, and major-axis tilt angle, $\theta_q$, of the 3rd, 5th, 7th and 9th harmonic orders emitted by a single-crystal graphene irradiated with a linearly-polarized driving field, as a function of the crystal's $\Gamma - K'$ axis rotation-angle, $\theta$. In both panels the crystal's orientation spans over $0<\theta<60°$ since, due to the graphene's symmetry, the pattern is repeated periodically for all subsequent angular intervals. Both parameters, $\epsilon_q$ and $\theta_q$, are basically unaffected for the lower-order harmonics, i.e. the lower-order harmonics are almost linearly polarized in the same direction as the driver. In contrast, the higher-order harmonics show a substantial deviation from the driver's polarization, as graphene's anisotropy is more pronounced for the highest orders in the HHG spectrum. Note also, in this latter case, that both ellipticity and major-axis tilt-angle show a maximum deviation from the driver's at orientation angles odd-multiples of $\theta = 15°$. In addition, the deviations are symmetric and opposite with respect to $\theta = 30°$ for any harmonic order.

As a consequence of the non-linear anisotropy in single-crystal graphene, the different domains in a polycrystal will radiate high-order harmonics with a distinctive polarization state, depending on their particular orientation. However, note that, for a sufficient number of grains in the polycrystal, the domain orientations will spread over 360° (see Fig. 1(d)). This, together with the opposite symmetry of the non-linear response shown in Figs. 2(b) and 2(c), leads to the expectation that the net polycrystal harmonic emission present the same polarization properties as the driving field. However, for finite-size polycrystals, similar to those in [3], the number of grains is limited to their cumulative area filling the polycrystal's surface. Therefore, in this case, we should expect a residual ellipticity and tilt deviations in the harmonics emitted by the target. Note that the magnitude of the residual deviations decreases progressively for polycrystals with large number of domains, as each realization will contain effectively all possible domain configurations. For the case of Fig. 1, as the number of domain configurations is 29000 and the mean domain size is 25 nm, this limit corresponds to polycrystals with sizes above 4.3 $\mu$m, about twice the size we are considering in this paper.

Optical Materials EXPRESS

Let us now consider the statistics of such deviations from repeated measurements of the polarization properties over a set of $N$ polycrystal realizations, grown accordingly to the same distribution of grains sizes and orientations. In particular, we focus into the mean and standard deviation of the tilt-angle and ellipticity of each $q$th-order harmonic, with respect to that of the driving field, which we assume linearly polarized in the vertical direction,

$$\langle \theta^q \rangle = \frac{1}{N}\sum_j^N \theta_j^q, \qquad \langle \epsilon^q \rangle = \frac{1}{N}\sum_j^N \epsilon_j^q \tag{8}$$

$$\sigma_\theta^q = \sqrt{\frac{1}{N}\sum_j^N \left(\theta_j^q - \langle \theta^q \rangle\right)^2}, \qquad \sigma_\epsilon^q = \sqrt{\frac{1}{N}\sum_j^N \left(\epsilon_j^q - \langle \epsilon^q \rangle\right)^2} \tag{9}$$

where $\theta_j^q$ and $\epsilon_j^q$ are the tilt angle and ellipticity of the $q$th-order harmonic radiated by the $j$ polycrystal realization. Consistently with the above discussion on the symmetries of single-crystal graphene's anisotropy, we find near vanishing results for the mean values in Eqs. (8), i.e. $\theta_q$ and $\epsilon_q$ are not sensitive enough to characterize the polycrystal domain distribution. In contrast, the standard deviations presented in Eqs. (9), $\sigma_\theta^q$ and $\sigma_\epsilon^q$, for the harmonic orders 3rd to 9th show non-vanishing values, as shown in Fig. 2(d). Note that while the deviations of the ellipticity are rather small, those of the harmonic tilt-angle are large enough to be measured for the higher harmonics. Therefore harmonic tilt-angle deviation is a potentially useful parameter for the characterization of polycrystal domain order.

In order to demonstrate the sensitivity of the standard deviation $\sigma_\theta^q$ to the domain-size distribution, we have performed a series of calculations of $\sigma_\theta^7$ for different Gaussian distributions, $\exp(-(s-s_0)^2/2\sigma^2)$, with $s_0$<1000 nm being the most frequent domain size and $\sigma$<360 nm. Figure 3(a) plots the results extracted from a set of $8\times10^4$ crystal realizations for each Gaussian distribution. The two insets in panel (a) represent two examples of domain distributions with $s_0$ = 500 nm and widths of 353.6 nm (upper inset, green) and 35.4 nm (lower inset, yellow). We find an approximate linear dependence of the tilt-angle standard deviation $\sigma_\theta^7$ with the grain size $s_0$, with slopes varying as a function of the polycrystal distribution width $\sigma$. In all cases, the variations in the standard deviation $\sigma_\theta^7$ with the distribution are of some tens of degrees, therefore sensitive enough to use this quantity in a polarimetric characterization of the distribution.

As a proof-of-concept, we finally propose a possible strategy for the characterization of the graphene polycrystal domain-size distribution based on high-order harmonic polarimetry. For this, we shall use Fig. 3(b), which shows the same information as Fig. 3(a) but representing the tilt-angle standard deviation $\sigma_\theta^7$ (color scale) as a function of $s_0$ and $\sigma$. We now consider an hypothetical experiment in which we measure the tilt angle of the 7th harmonic, $\theta_j^7$, for a set of $j \in N$ polycrystals, fabricated under similar conditions, and thus according to the same domain-size distribution. We compute the standard deviation of the measurements $\sigma_\theta^7\big|_{meas}$ according to Eq. (9). For concreteness, we have run a simulation of this hypothetical experiment using the distribution shown in Figs. 1(b) and 1(c), similar to that reported in [3], from which we obtain a value of $\sigma_\theta^7\big|_{meas} = 7.4°$. Knowing the value of $\sigma_\theta^7\big|_{meas}$, we choose the corresponding contour in Fig. 3(b) to find the relation between the grain-distribution width $\sigma$ in terms of the most frequent size $s_0$. This contour predicts a width of $\sigma_{exp}$ = 264.3 nm for $s_0$ = 25 nm, i.e. the most frequent size in the distribution of Figs. 1(b). The corresponding Gaussian profile is plotted in Fig. 1(b) as a solid black line. We confirm the accuracy of our method comparing $\sigma_{exp}$ with the best Gaussian profile fit of the histograms in Fig. 1(b), which leads to the value of 275.8 nm.

In order to demonstrate the robustness of our procedure, in Fig. 3(c) we represent the corresponding contours resulting from the same road map applied to drivers with different intensities, from $3.5\times10^{10}$ W/cm$^2$ to $1.14\times10^{11}$ W/cm$^2$, and considering both the 7th and 9th harmonic-orders. The excellent overlapping of the contours reveals an extraordinary consistency

Optical Materials EXPRESS

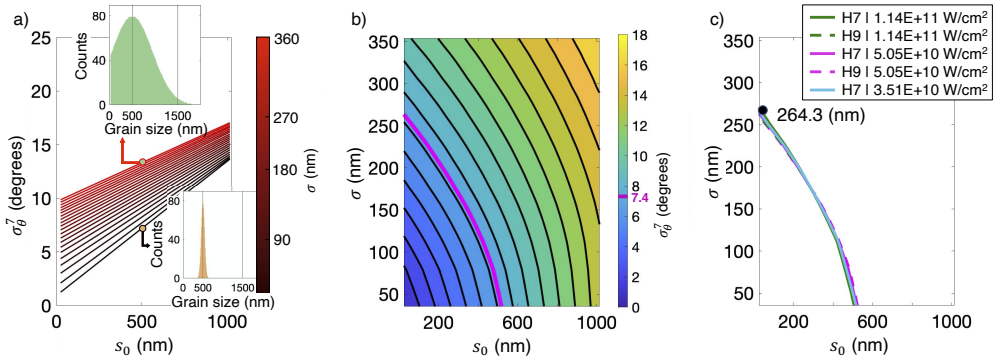


**Fig. 3.** a) Standard deviation of the 7th harmonic tilts $\sigma_\theta^7$ computed for different Gaussian distributions of grain sizes, from wider (red light line) to narrower (red dark line). The insets show the Gaussian distributions for the wider case (green dot) and the narrower case (orange dot), respectively, centered at $s_0 = 500$ nm grain size. b) dependence of the tilt angle deviation $\sigma_\theta^7$ in terms of the width $\sigma$ and the most frequent size $s_0$ of the Gaussian distribution, the magenta line corresponds to all the contour $\sigma_\theta^7 = 7.4°$. Both a) and b) panels correspond to a driver of intensity of $5.1 \times 10^{11} W/cm^2$. c) shows the contours found for different driving intensities, from $3.5 \times 10^{10}$ W/cm$^2$ to $1.14 \times 10^{11}$ W/cm$^2$, and for harmonics 7th an 9th.

in the prediction of domain-size standard deviations using different drivers and harmonic orders. We believe that this result demonstrates the reliability of HHG polarimetry for the characterization of polycrystaline graphene.

## 4. Conclusion

We have proposed high-order harmonic polarimetry as a method for the characterization of domain parameters in single-layer graphene polycrystals. Our proposal stems from the recently reported non-linear anisotropy in single-crystal graphene. While our theoretical simulations show that the efficiency of high-order harmonic generation in polycrystals, as well as the ellipticity measurements, are not sensitive enough to the details of the polycrystal disorder, we demonstrate that the measurement of the tilt angle is indeed sensitive. As a proof-of-principle, we suggest a simple method to retrieve the width of the grain-size distribution from the statistical deviation of the measurements of the tilt rotation of the harmonics for a set of polycrystal realizations.

**Funding.** European Research Council (8511201); Ministerio de Educación y Formación Profesional (FPU18/03348); Junta de Castilla y León (SA287P18); Ministerio de Ciencia, Innovación y Universidades (PID2019-106910GB-100, RYC-2017-22745).

**Acknowledgments.** We acknowledge support from the European Research Council (ERC) under the European Union's Horizon 2020 research and innovation programme (grant agreement No. 851201).

**Disclosures.** The authors declare no conflicts of interest.

**Data availability.** Data underlying the results presented in this paper are not publicly available at this time but may be obtained from the authors upon reasonable request.

## References

1. S. K. Tiwari, S. Sahoo, N. Wang, and A. Huczko, "Graphene research and their outputs: Status and prospect," J. Sci.: Adv. Mater. Devices **5**, 10–29 (2020).
2. M. Saeed, Y. Alshammari, S. A. Majeed, and E. Al-Nasrallah, "Chemical vapour deposition of graphene-synthesis, characterisation, and applications: A review," Molecules **25**(17), 3856 (2020).

Optical Materials EXPRESS


3. P. Y. Huang, C. S. Ruiz-Vargas, A. M. van der Zande, W. S. Whitney, M. P. Levendorf, J. W. Kevek, S. Garg, J. S. Alden, C. J. Hustedt, Y. Zhu, J. Park, P. L. McEuen, and D. A. Muller, "Grains and grain boundaries in single-layer graphene atomic patchwork quilts," Nature **469**(7330), 389–392 (2011).
4. B. G. Mendis, Q. M. Ramasse, T. P. Shalvey, J. D. Major, and K. Durose, "Optical properties and dielectric functions of grain boundaries and interfaces in cdte thin-film solar cells," ACS Appl. Energy Mater. **2**(2), 1419–1427 (2019).
5. W. Zhao, B. Xia, and L. L. , *et al.*, "Low-energy transmission electron diffraction and imaging of large-area graphene," Sci. Adv. **3**(9), e1603231 (2017).
6. Z. Ni, Y. Wang, T. Yu, and Z. Shen, "Raman spectroscopy and imaging of graphene," Nano Res. **1**(4), 273–291 (2008).
7. T. Popmintchev, M. C. Chen, and D. P. et al, "Bright coherent ultrahigh harmonics in the kev x-ray regime from mid-infrared femtosecond lasers," Science **336**(6086), 1287–1291 (2012).
8. X. Shi, C.-T. Liao, Z. Tao, E. Cating-Subramanian, M. M. Murnane, C. Hernández-García, and H. C. Kapteyn, "Attosecond light science and its application for probing quantum materials," J. Phys. B: At., Mol. Opt. Phys. **53**(18), 184008 (2020).
9. A. McPherson, G. Gibson, H. Jara, U. Johann, T. S. Luk, I. A. McIntyre, K. Boyer, and C. K. Rhodes, "Studies of multiphoton production of vacuum-ultraviolet radiation in the rare gases," J. Opt. Soc. Am. B **4**(4), 595–601 (1987).
10. M. Ferray, A. L'Huillier, X. F. Li, L. A. Lompre, G. Mainfray, and C. Manus, "Multiple-harmonic conversion of 1064 nm radiation in rare gases," J. Phys. B: At. Mol. Opt. Phys. **21**(3), L31–L35 (1988).
11. S. Ghimire and D. A. Reis, "High-harmonic generation from solids," Nat. Phys. **15**(1), 10–16 (2019).
12. K. J. Schafer, B. Yang, L. F. DiMauro, and K. C. Kulander, "Above threshold ionization beyond the high harmonic cutoff," Phys. Rev. Lett. **70**(11), 1599–1602 (1993).
13. N. Tancogne-Dejean and A. Rubio, "Atomic-like high-harmonic generation from two-dimensional materials," Sci. Adv. **4**(2), eaao5207 (2018).
14. A. García-Cabrera, C. Hernández-García, and L. Plaja, "Ultrafast sub-nanometer matter-wave temporal talbot effect," New J. Phys. **23**(9), 093011 (2021).
15. G. Vampa, C. R. McDonald, G. Orlando, D. D. Klug, P. B. Corkum, and T. Brabec, "Theoretical analysis of high harmonic generation in solids," Phys. Rev. Lett. **113**(7), 073901 (2014).
16. G. Vampa, T. J. Hammond, N. Thiré, B. E. Schmidt, F. Légaré, C. R. McDonald, T. Brabec, and P. B. Corkum, "Linking high harmonics from gases and solids," Nature **522**(7557), 462–464 (2015).
17. L. Yue and A. M. B. Gaarde, "Imperfect recollisions in high-harmonic generation in solids," Phys. Rev. Lett. **124**(15), 153204 (2020).
18. R. Boyero-García, A. García-Cabrera, O. Zurrón-Cifuentes, C. Hernández-García, and L. Plaja, "Non-classical high harmonic generation in graphene driven by linearly-polarized laser pulses," Opt. Express **30**(9), 15546–15555 (2022).
19. O. Zurrón, A. Picón, and L. Plaja, "Theory of high-order harmonic generation for gapless graphene," New J. Phys. **20**(5), 053033 (2018).
20. O. Zurrón-Cifuentes, R. Boyero-García, C. Hernández-García, and L. Plaja, "High harmonic generation in armchair carbon nanotubes," Opt. Express **28**, 719760 (2020).
21. J. Li, J. Lu, A. Chew, S. Han, J. Li, Y. Wu, H. Wang, S. Ghimire, and Z. Chang, "Attosecond science based on high harmonic generation from gases and solids," Nat. Commun. **11**(1), 2748 (2020).
22. O. Schubert, M. Hohenleutner, F. Langer, B. Urbanek, C. Lange, U. Huttner, D. Golde, T. Meier, M. Kira, S. W. Koch, and R. Huber, "Sub-cycle control of terahertz high-harmonic generation by dynamical bloch oscillations," Nat. Photon. **8**(2), 119–123 (2014).
23. N. Tancogne-Dejean, O. D. Mücke, F. X. Kärtner, and A. Rubio, "Impact of the electronic band structure in high-harmonic generation spectra of solids," Phys. Rev. Lett. **118**(8), 087403 (2017).
24. Y. S. You, D. A. Reis, and S. Ghimire, "Anisotropic high-harmonic generation in bulk crystals," Nat. Phys. **13**(4), 345–349 (2017).
25. H. Liu, Y. Li, Y. You, S. Ghimire, T. F. Heinz, and D. A. Reis, "High-harmonic generation from an atomically thin semiconductor," Nat. Phys. **13**(3), 262–265 (2017).
26. N. Yoshikawa, T. Tamaya, and K. Tanaka, "High-harmonic generation in graphene enhanced by elliptically polarized light excitation," Science **356**(6339), 736–738 (2017).
27. O. Zurrón-Cifuentes, R. Boyero-García, C. Hernández-García, A. Picón, and L. Plaja, "Optical anisotropy of non-perturbative high-order harmonic generation in gapless graphene," Opt. Express **27**(5), 7776–7786 (2019).
28. Z.-Y. Chen and R. Qin, "Circularly polarized extreme ultraviolet high harmonic generation in graphene," Opt. Express **27**(3), 3761–3770 (2019).
29. N. Klemke, N. Tancogne-Dejean, G. M. Rossi, Y. Yang, F. Scheiba, R. E. Mainz, G. Di Sciacca, A. Rubio, F. X. Kärtner, and O. D. Mucke, "Polarization-state-resolved high-harmonic spectroscopy of solids," Nat. Commun. **10**(1), 1319 (2019).
30. L. Zhou, H. Fu, T. Lv, C. Wang, H. Gao, D. Li, L. Deng, and W. Xiong, "Nonlinear optical characterization of 2d materials," Nanomaterials **10**(11), 2263 (2020).
31. M. S. Mrudul, "High-harmonic spectroscopy of two-dimensional materials," Ph.D. thesis, Indian Institute of Technology, Bombay (2021).
32. S. Reich, C. Thomsen, and J. Maultzsch, *Carbon Nanotubes: Basic Concepts and Physical Properties* (Wiley-VCH, 2004).